Supporting Information for

Time-resolved EPR observation of blue-light-induced radical ion pairs in a flavin–Trp dyad

Yoshimi Oka*[abc] and Katsuya Inoue [c]

[a.] *Frontier Research Core for Life Sciences, University of Toyama, 2630 Sugitani, Toyama 930-0194, Japan.*

[b.] *Research Promotion Institute, Oita University, 700 Dannoharu, Oita 870-1192, Japan.*

[c.] *International Institute for Sustainability with Knotted Chiral Meta Matter (WPI–SKCM^2), Chirality Research Center (CResCent) and Graduate School of Advanced Science and Engineering, Hiroshima University, 1-3-1 Kagamiyama, Higashihiroshima 739-8526, Japan.*

Contents

1. Synthesis	S2
2. Crystal structure	S10
3. Absorption and fluorescence spectra	S15
4. Fluorescence quantum yields	S17
5. Fluorescence decay curves	S18
6. Concentration-dependency of fluorescence intensity	S20
7. Temperature dependence of fluorescence quenching	S21
8. TREPR spectra	S23
9. Titration experiments of FlH–MB with tryptophan methyl ester	S26
10. DFT calculations	S28
11. References	S30

1. Synthesis

All chemicals and solvents were purchased from Aldrich, TCI, Wako or Nacalai, and used as received without further purification.

Scheme S1. A synthetic route to **1**.

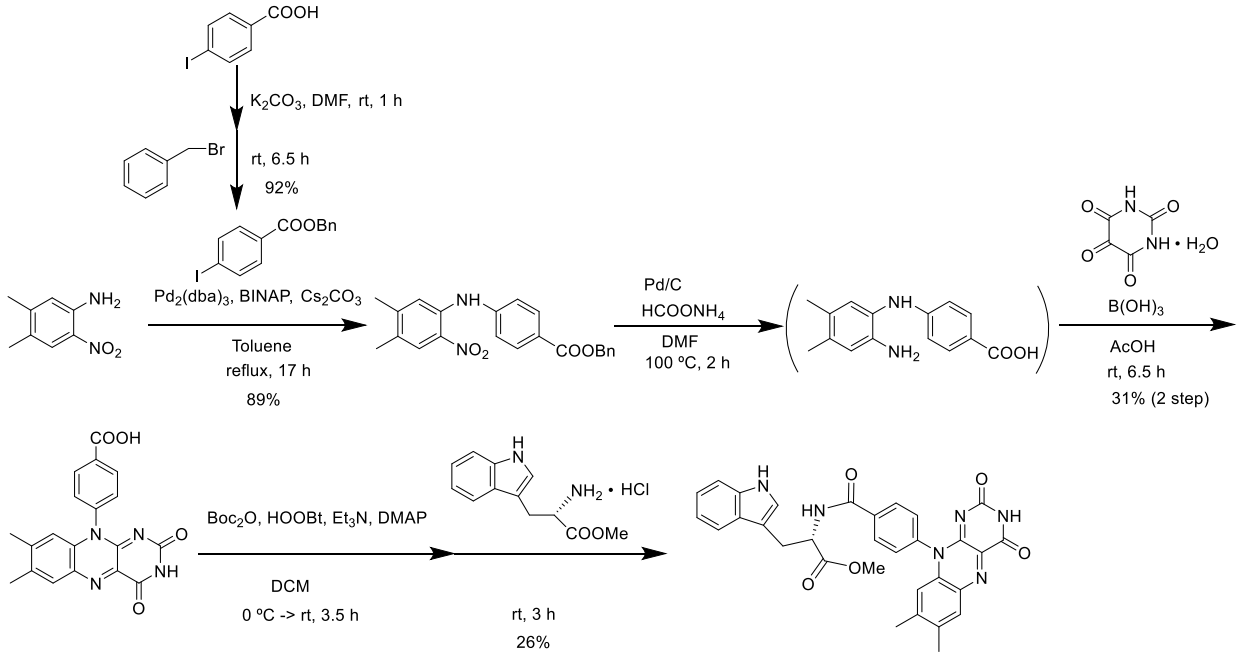

4-Iodobenzoic acid benzyl ester.

To 4-iodobenzoic acid (15.6 g, 63 mmol) in anhydrous DMF (90 mL), K_2CO_3 (8.7 g, 0.063 mmol) was added and the suspension was stirred for 1 h. Then the benzyl bromide (7.2 mL, 61 mmol) was instilled over 5 min, and the resulting suspension was stirred under nitrogen atmosphere at room temperature. After stirring 6.5 h, the solvent was distilled off under reduced pressure and the mixture was poured into water and extracted with Et_2O. The organic phase was washed with water and brine, dried with $MgSO_4$, evaporated and concentrated under vacuum. 4-iodobenzoic acid benzyl ester was obtained as a white crystalline solid (18.9 g, 56 mmol, 92% yield). ^{1}H NMR (500 MHz, DMSO-d_6, 29 °C): δ = 7.92 (dd, J = 8.4, 1.8 Hz, 2H), 7.74 (dd, J = 8.4, 1.8 Hz, 2H), 7.47 (d, J = 7.1 Hz, 2H), 7.34-7.42 (m, 3H), 5.35 ppm (s, 2H); ^{13}C NMR (125.7 MHz, DMSO-d_6, 22 °C): δ = 165.1, 137.7, 135.8, 130.8, 128.9, 128.4, 128.1, 127.9, 101.8, 66.3 ppm.

4-((4,5-Dimethyl-2-nitrophenyl)amino)benzoic acid benzyl ester.

A mixture of 4,5-dimethyl-2-nitroaniline (4.5 g, 27 mmol) and 4-iodobenzoic acid benzyl ester (9.3 g, 27 mol) in anhydrous toluene (80 mL) was stirred under nitrogen atmosphere at room temperature. After adding $Pd_2(dba)_3$ (tris(dibenzylideneacetone)dipalladium(0), 1.3 g, 1.4 mmol), (±)-BINAP (2,2'-bis(diphenylphosphino)-1,1'-binaphthyl, 1.3 g, 2.1 mmol) and Cs_2CO_3 (12.4 g, 38 mmol), the resulting suspension was heated to reflux and maintained for 17 h. Then the reaction solution was cooled to room temperature and filtered through Celite, and the Celite was rinsed with EtOAc. Subsequently, the organic phase was washed with water and brine, dried with $MgSO_4$, and evaporated in vacuo. 4-((4,5-dimethyl-2-nitrophenyl)amino)benzoic acid benzyl ester was purified by chromatography on silica gel with CH_2Cl_2 and obtained as an orange solid (8.9 g, 24 mmol, 89%yield). ^{1}H NMR (500 MHz, DMSO-d_6, 29 °C): δ = 9.19 (s, 1H), 7.89-7.94 (m, 3H), 7.46 (d, J = 7.1 Hz, 2H), 7.40-7.43 (m, 2H), 7.32 (s, 1H), 7.26 (dd, J = 8.8, 2.0 Hz, 2H), 7.21 (br s, 1H), 5.32 (s, 2H), 2.24 ppm (s, 6H); ^{13}C NMR (125.7 MHz, DMSO-d_6, 22 °C): δ = 165.1, 146.2, 145.8, 136.3, 135.8, 135.5, 130.8, 130.3, 128.4, 127.9, 127.8, 125.8, 124.4, 122.1, 121.0, 118.9, 118.2, 65.7, 19.6, 18.2 ppm; EI-MS: m/z calcd for $C_{22}H_{20}N_2O_4$ 376, found 376.

4-(7',8'-Dimethylisoalloxazin-10'-yl)benzoic acid.

To 4-((4,5-dimethyl-2-nitrophenyl)amino)benzoic acid benzyl ester (1.0 g, 2.7 mmol) in anhydrous DMF (20 mL) was added $HCOONH_4$ (0.9 g, 14 mmol) and 10% Pd/C (0.3 g, 0.28 mmol) and the suspension was stirred under nitrogen atmosphere at room temperature. Then the reaction was heated to 100 °C and maintained for 2 h, when the starting material was consumed as determined by TLC (eluent: Hex/EtOAc = 3/1). After cooling to room temperature, the reaction solution was filtered through Celite using CH_2Cl_2. The organic phase was washed with water, dried with $MgSO_4$, and evaporated in vacuo. The reduction product of brown solution including small amount of DMF was allowed to use for the following reaction without further purification. To the reduction product dissolved in AcOH (20 mL) was added $B(OH)_3$ (3.3 g, 53 mmol) and alloxan monohydrate (1.7 g, 11 mmol), and then the reaction mixture was stirred at room temperature for 6h. The reaction proceeded with color change of solution from yellow to fluorescent yellow green and precipitation of powder. The powder was filtered, collected, washed with water and dried in vacuo. 4-(7',8'-dimethylisoalloxazin-10'-yl)benzoic acid was obtained as a yellow green powder (0.3 g, 0.85 mmol, 31%yield). ^{1}H NMR (500 MHz, DMSO-d_6, 29 °C): δ = 11.32 (s, 1H), 8.22 (d, J = 8.4, 2H), 7.97 (s, 1H), 7.49 (d, J = 8.4 Hz, 2H), 6.57 (s, 1H) , 2.38 (s, 3H) , 2.28 ppm (s, 3H); ^{13}C NMR (125.7 MHz, DMSO-d_6, 22 °C): δ = 179.1, 159.6, 155.3, 151.3, 138.0, 135.7, 133.6, 132.0, 131.0, 130.6, 127.8,

116.3, 20.4, 18.7; ESI-MS: *m*/*z* calcd for $C_{19}H_{14}N_4O_4$ $[M + H]^+$: 363.11, found: 363.11; $[M + Na]^+$: 385.09, found: 385.09; $[M + K]^+$: 401.06, found: 401.07.

(*S*)-2-Amino-N$^{\alpha}$-(4-(7',8'-dimethylisoalloxazin-10'-yl)phenylcarbonyl)-3-(1H-indol-3-yl)propanoic acid methyl ester.

The reaction was referred to the reported activation method for carboxylic acid.[1] To BOC_2O (di-*tert*-butyl dicarbonate, 0.24 g, 0.92 mmol) in anhydrous CH_2Cl_2 (20 mL) was added 4-(7',8'-dimethylisoalloxazin-10'-yl)benzoic acid (0.28 g, 0.77 mmol), HODhbt (3-hydroxy-3,4-dihydrobenzotriazine-4-one, 0.13 g, 0.80 mmol), Et_3N(0.2 mL, 1.4 mmol) and DMAP (4-dimethylaminopyridine, 0.06 g, 0.49 mmol) under nitrogen atmosphere at 0 °C. The reaction mixture was stirred and heated to room temperature. After 3.5 h, (*S*)-TrpOMe·HCl (L-tryptophan methyl ester hydrochloride, 0.24 g, 0.94 mmol) was added, and the reaction was allowed to proceed for 3 h. To the resulting solution, CH_2Cl_2 was added and the solution was washed with 2% HCl, saturated $NaHCO_3$ solution and water, dried with $MgSO_4$ and evaporated. (*S*)-2-Amino-N$^{\alpha}$-(4-(7',8'-Dimethylisoalloxazin-10'-yl)phenylcarbonyl)-3-(1H-indol-3-yl) propanoic acid methyl ester was precipitated as an orange powder from $CHCl_3$ solution, filtered, collected and dried. (0.11 g, 0.20 mmol, 26% yield). ^{1}H NMR (500 MHz, DMSO-d_6, 29 °C): δ = 11.33 (s, 1H), 10.85 (br s, 1H), 9.06 (d, *J* = 7.6 Hz, 1H), 8.06-8.8.15 (m, 2H), 7.97 (s, 1H), 7.59(d, *J* = 7.9 Hz, 1H), 7.52 (dd, *J* = 8.1, 2.3 Hz, 2H), 7.34 (d, *J* = 8.1 Hz, 1H), 7.26 (d, *J* = 2.1 Hz, 1H), 6.99-7.10 (m, 2H), 6.56 (s, 1H), 4.77 (m, 1H), 3.68 (s, 3H), 3.20-3.40 (2H*, not clear because of overlapping with H_2O peak), 2.38 (s, 3H), 2.28 ppm (s, 3H); ^{13}C NMR (125.7 MHz, DMSO-d_6, 22 °C): δ = 179.1, 172.3, 165.7, 159.6, 155.3, 151.3, 146.2, 138.5, 137.9, 136.0, 135.8, 134.9, 133.5, 131.9, 129.4, 129.3, 127.9, 127.0, 123.6, 120.9, 118.4, 117.9, 116.3, 111.4, 109.8, 53.8, 51.9, 26.5, 20.3, 18.7 ppm; ESI-MS: *m*/*z* calcd for $C_{31}H_{26}N_6O_5$ $[M + H]^+$: 563.20, found: 563.20; $[M + Na]^+$: 585.19, found: 585.19.

*To identify the compound, additional ^{1}H NMR measurement using CD_3CN was performed. ^{1}H NMR (500 MHz, CD_3CN, 29 °C): δ = 9.18 (br s, 2H), 7.99-8.04 (m, 2H), 7.95 (s, 1H), 7.61 (d, *J* = 7.9 Hz, 1H), 7.35-7.42 (m, 4H), 7.19 (d, *J* = 2.4 Hz, 1H), 7.05-7.16 (m, 2H), 6.67 (s, 1H), 4.93-4.98 (m, 1H), 3.71 (s, 3H), 3.31-3.47 (m, 2H*), 2.40 (3H), 2.30 ppm (3H).

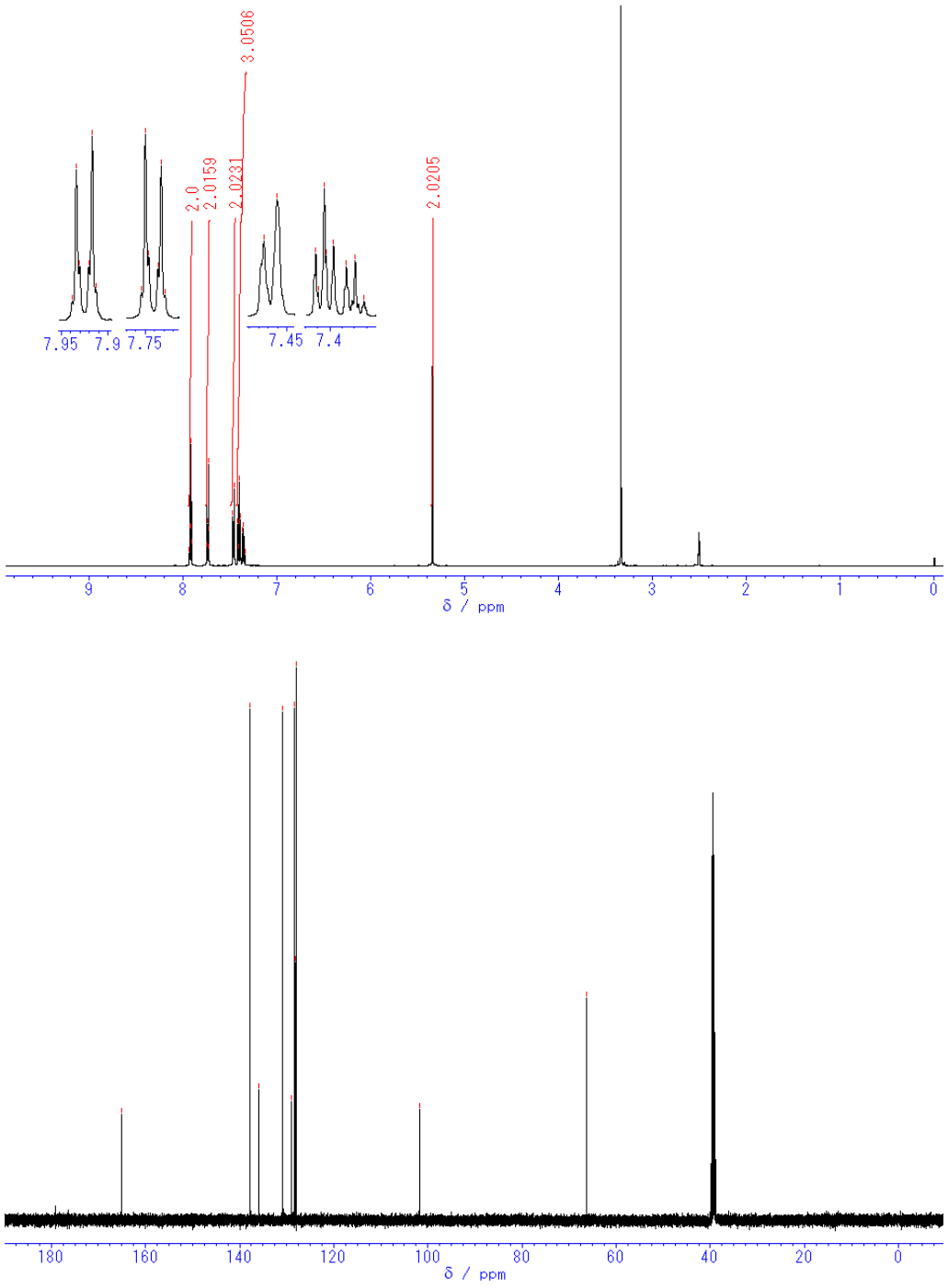

Fig. S1 ^{1}H and ^{13}C NMR spectra for 4-iodobenzoic acid benzyl ester.

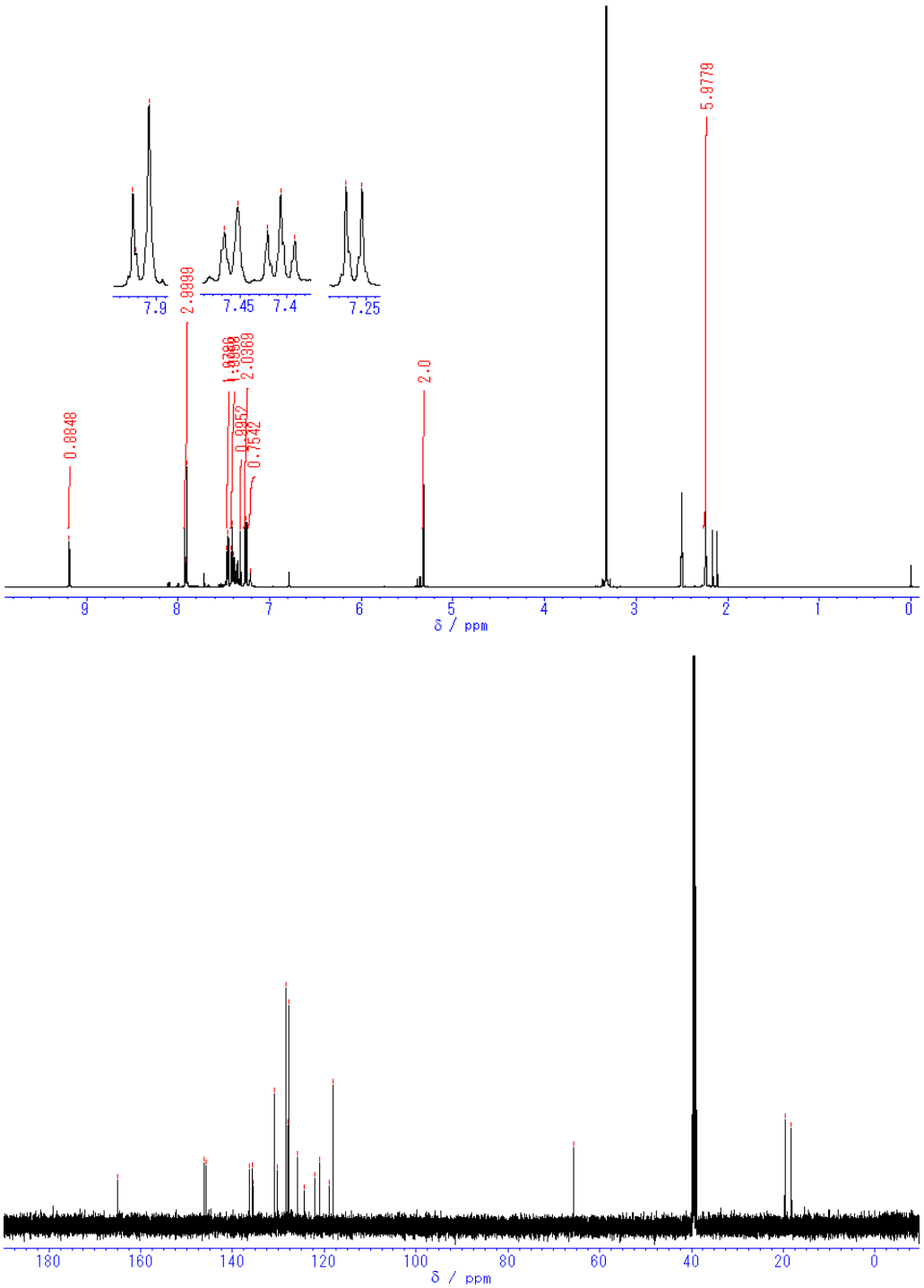

Fig. S2 ^{1}H and ^{13}C NMR spectra for 4-((4,5-dimethyl-2-nitrophenyl)amino)benzoic acid benzyl ester.

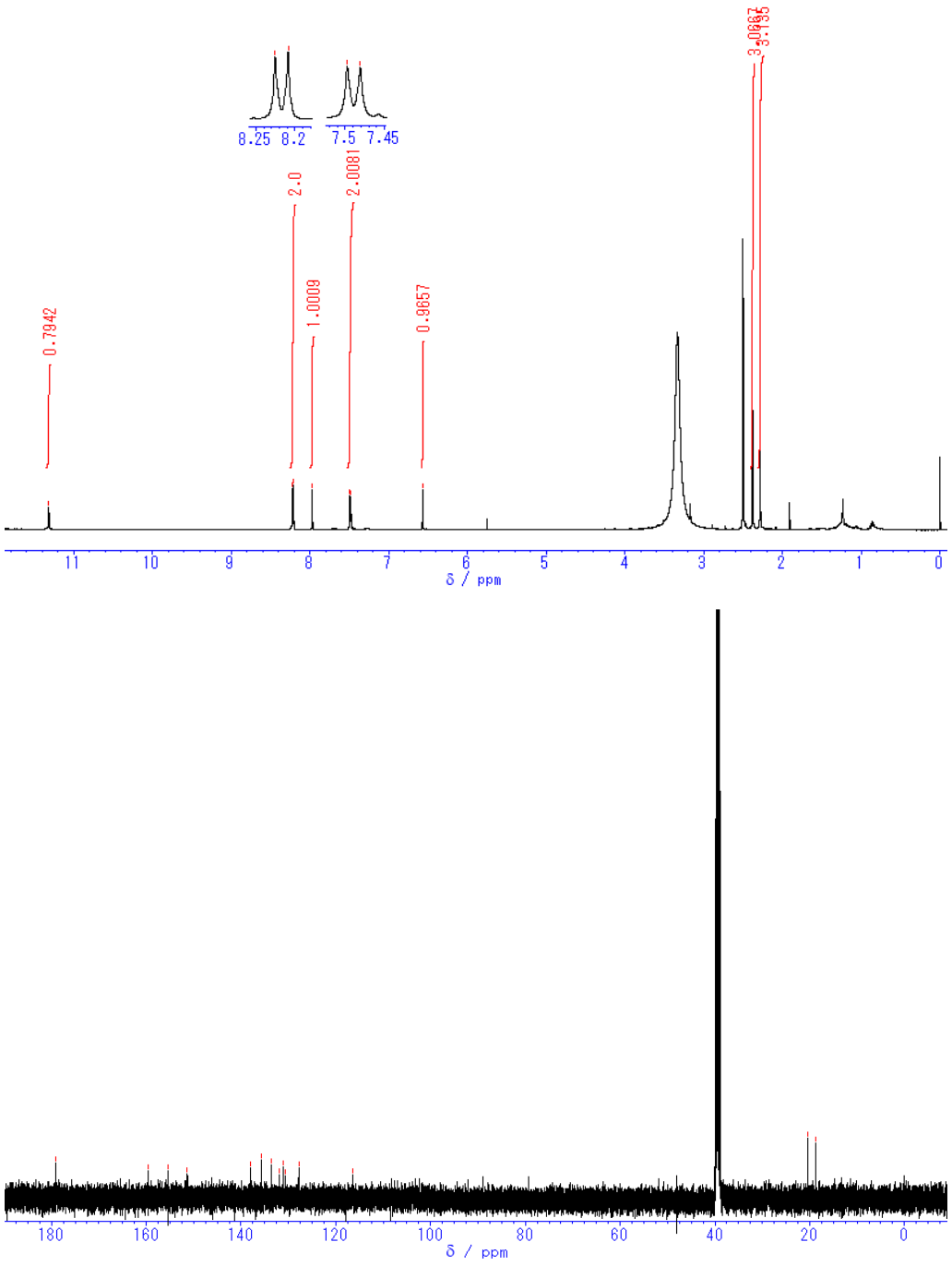

Fig. S3 ^{1}H and ^{13}C NMR spectra for 4-(7',8'-dimethylisoalloxazin-10'-yl)benzoic acid.

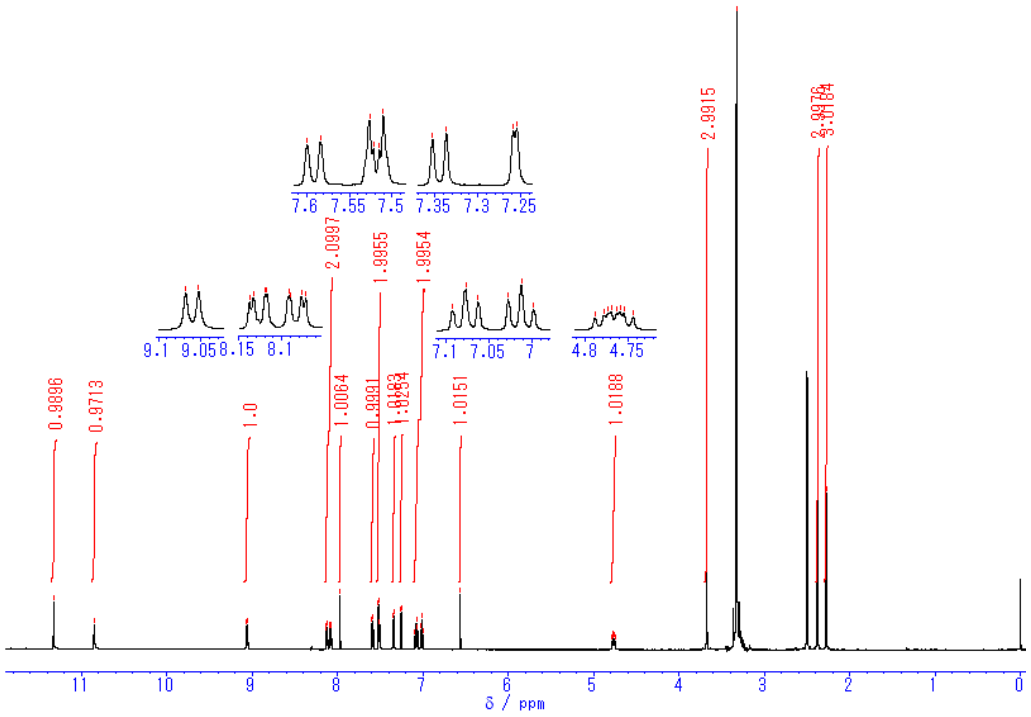
7.6 7.55 7.5
7.35 7.3 7.25
9.1 9.05 8.15 8.1
7.1 7.05 7
4.8 4.75
2.0997
1.9955
1.9954
2.9915
0.9896
0.9713
1.0
1.0064
1.0151
1.0188
11 10 9 8 7 6 5 4 3 2 1 0
δ / ppm

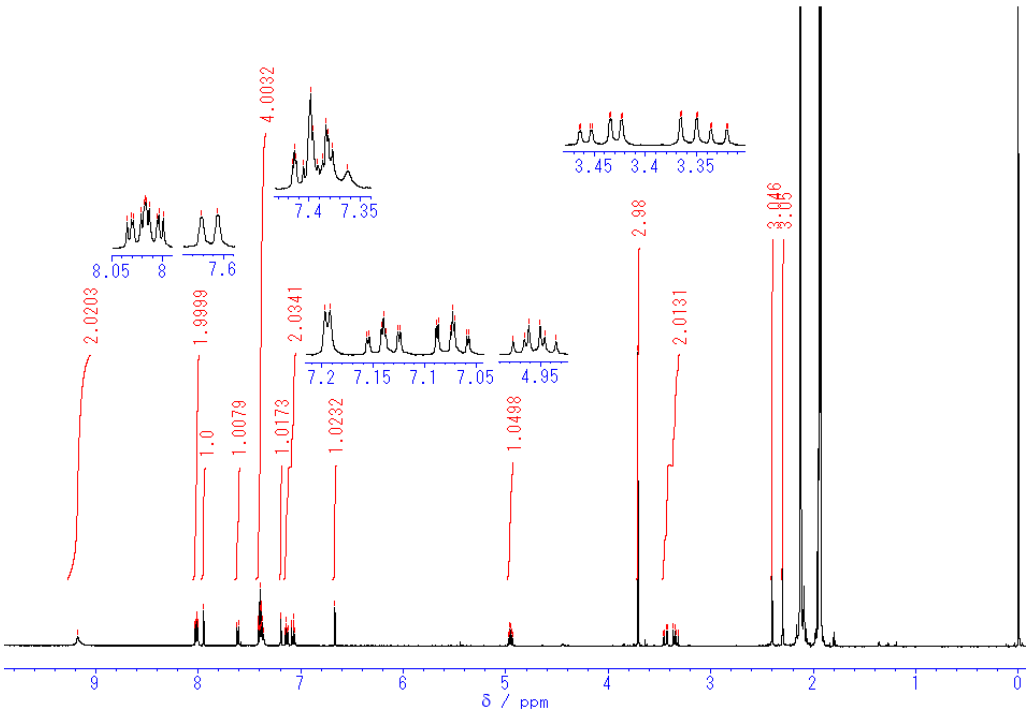
4.0032
7.4 7.35
3.45 3.4 3.35
8.05 8 7.6
2.0203
1.9999
2.0341
7.2 7.15 7.1 7.05
4.95
2.98
2.0131
1.0
1.0079
1.0173
1.0232
1.0498
9 8 7 6 5 4 3 2 1 0
δ / ppm

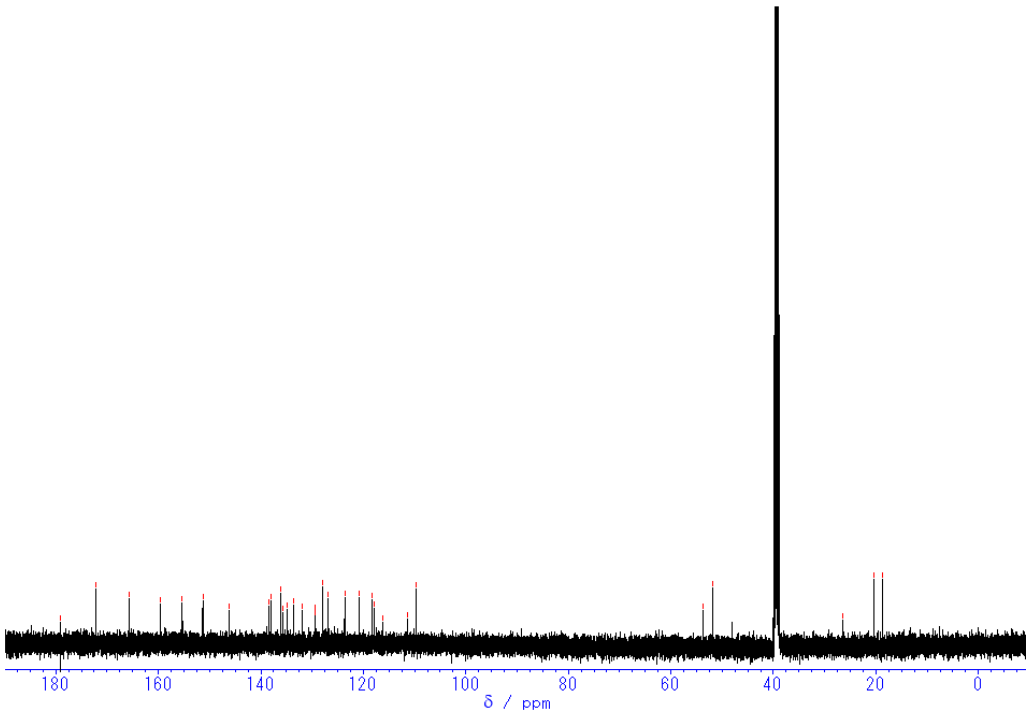

Fig. S4 ^{1}H and ^{13}C NMR spectra for (*S*)-2-amino-N$^{\alpha}$-(4-(7',8'-dimethylisoalloxazin-10'-yl)phenylcarbonyl)-3-(1H-indol-3-yl)propanoic acid methyl ester. Top: ^{1}H, DMSO-d_6; center: ^{1}H, CD_3CN; bottom: ^{13}C, DMSO-d_6.

2. Crystal structure

Crystallographic data (T = 173 K, radiation Cu-Kα = 1.54178 Å).

1: $C_{37}H_{45}N_6O_{8.5}S_3$; M = 805.97; crystal system: triclinic; space group: P1 (no. 1); a = 11.5061(2), b = 13.0272(2), c = 14.0938(2) Å; α = 72.4941(7), β = 84.3059(8), γ = 81.3692(7)°; V = 1988.62(5) Å^3; Z = 2; Dc = 1.346 g cm^{-3}; μ = 2.201 mm^{-1}; F(000) = 850; 3.293° ≤ θ ≤ 68.283°; hkl limits: -13/13, -15/15, -16/16; number of data measured: 45924; number of data with I = 2σ(I): 12256; R = 0.0614. Absolute structure parameter: 0.067(7). CCDC 2153389.

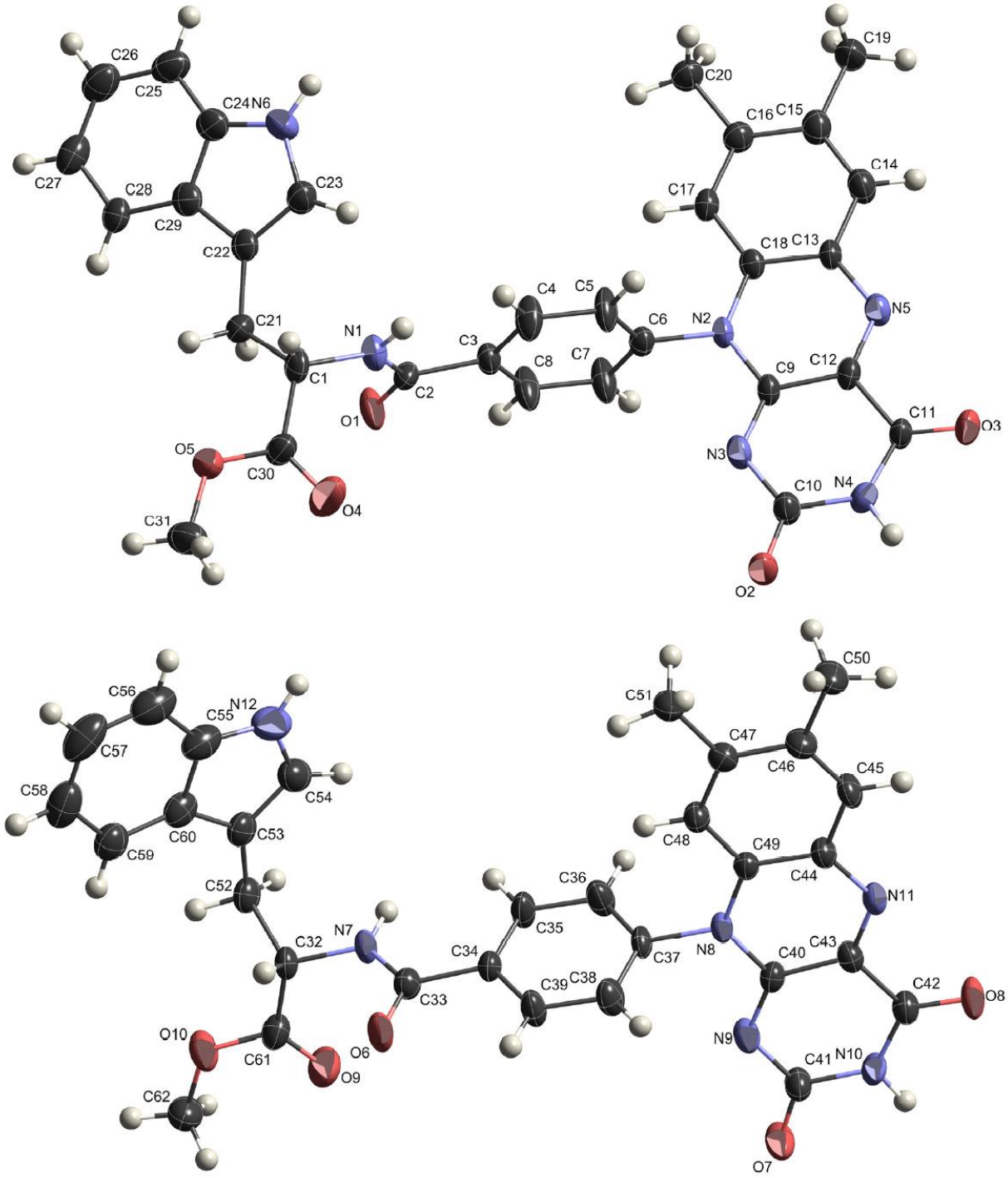

Fig. S5 Thermal ellipsoidal model of main molecules (two conformers) with atom labels. The ellipsoids are drawn at 50% probability level while isotropic hydrogen atoms are represented by spheres of arbitrary size.

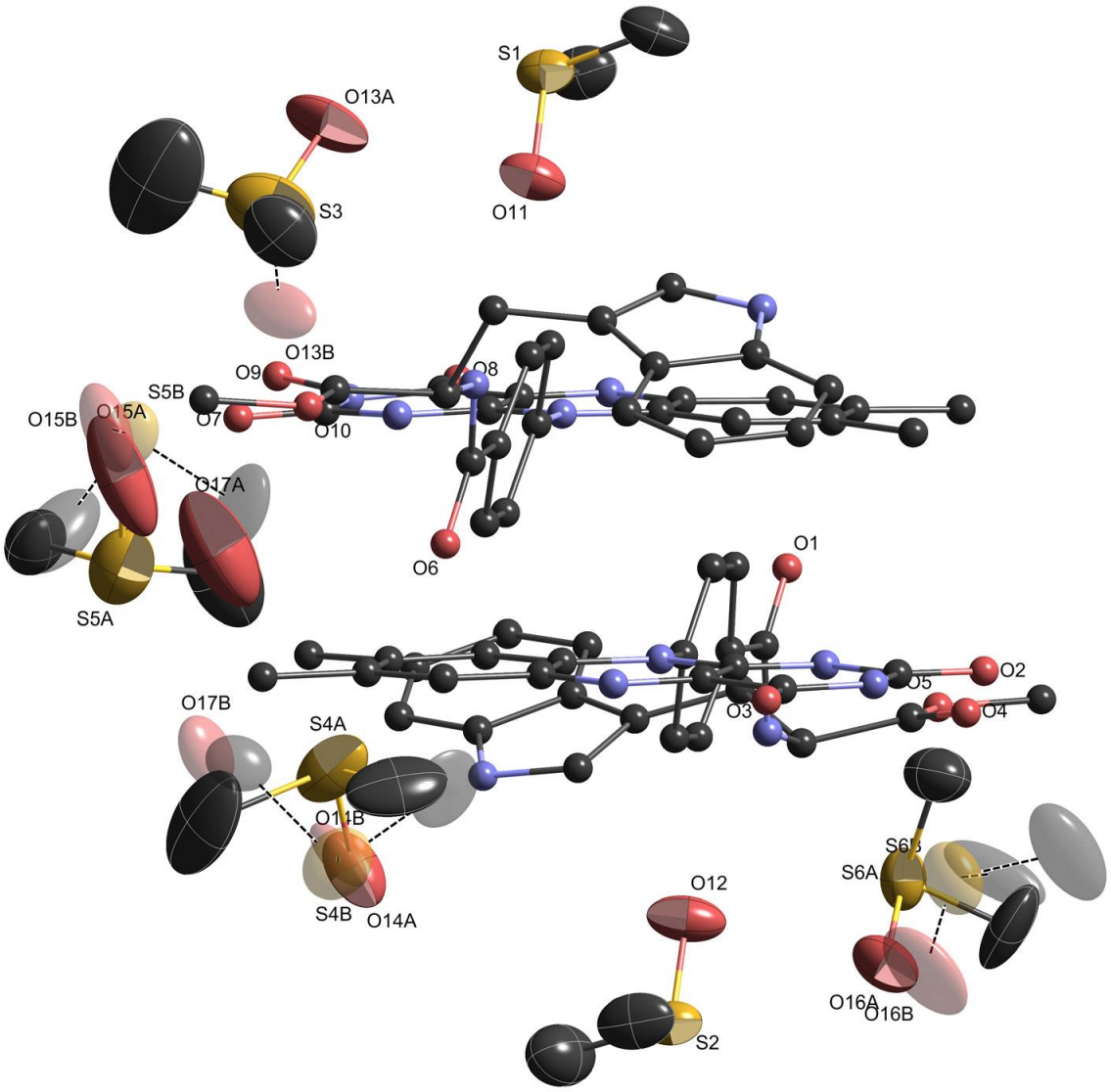

Fig. S6 Thermal ellipsoidal model of included solvent molecules (DMSO and water) with atom labels. The ellipsoids are drawn at 50% probability level. The main molecules are indicated with ball-and-stick model. The hydrogen atoms and labels of carbon atoms are omitted for clarity. Disordered atoms are colored transparently.

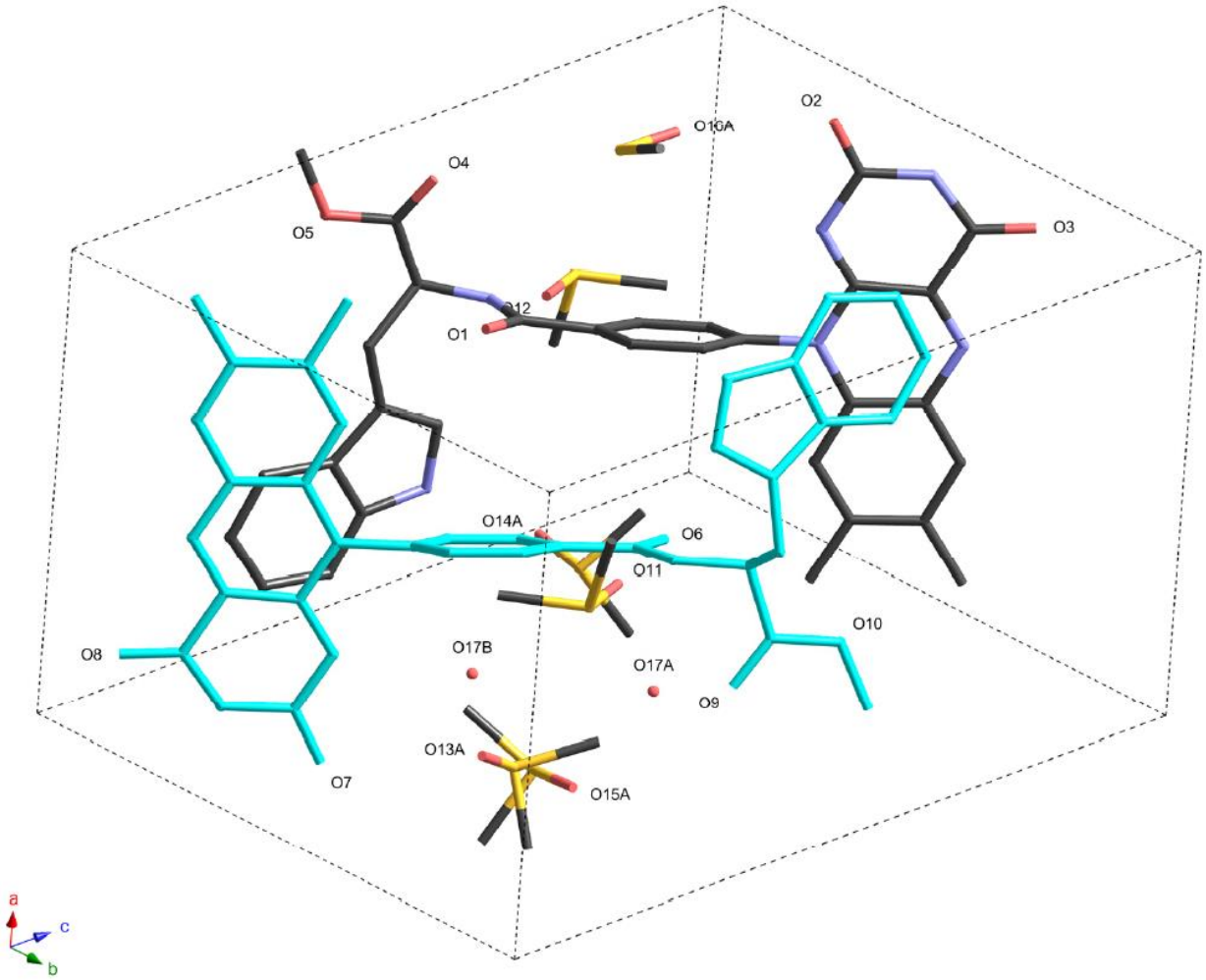

Fig. S7 Packing structure indicated by stick model. Hydrogen atoms and disordered atoms are omitted for clarity. One conformer is colored cyan.

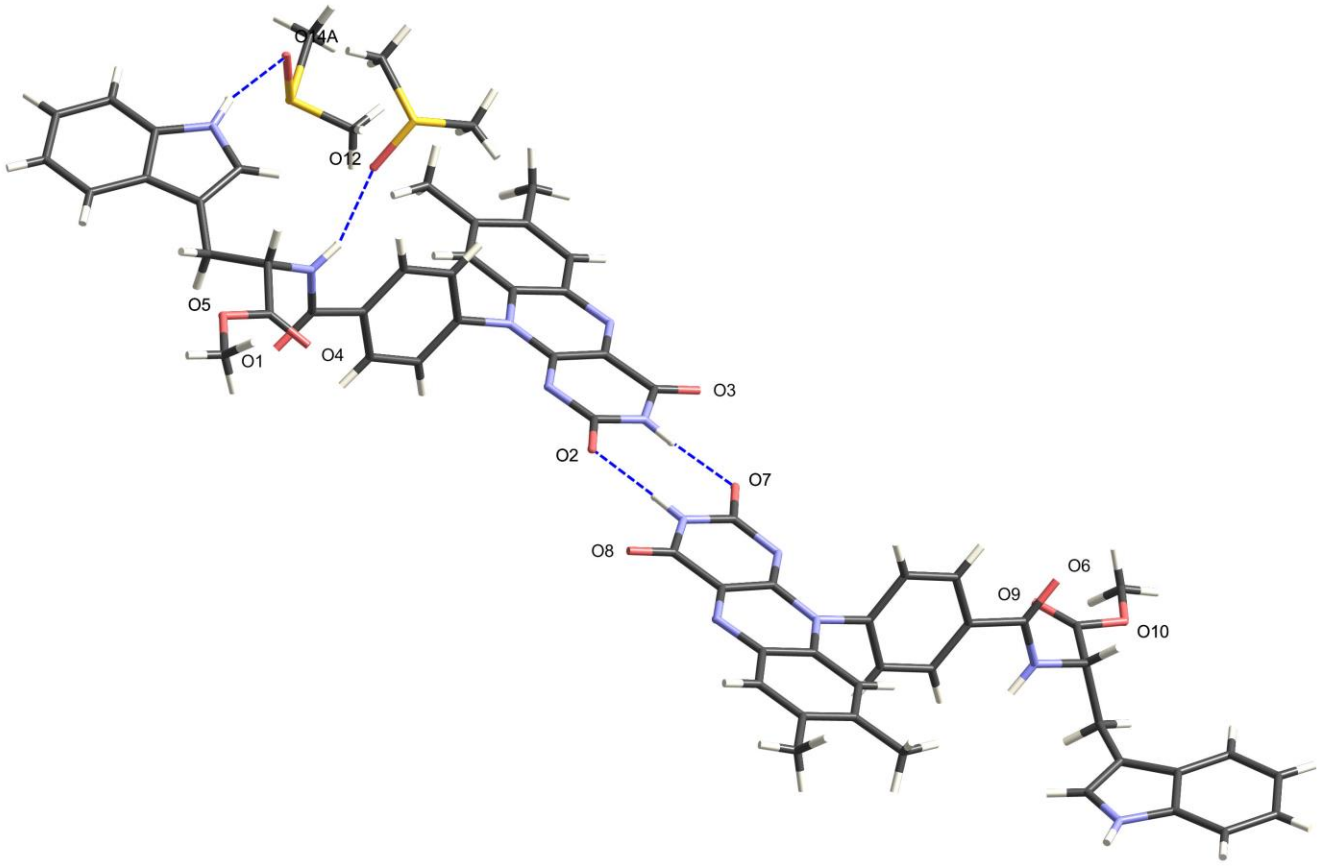

Fig. S8 Hydrogen bonding network in the crystal.

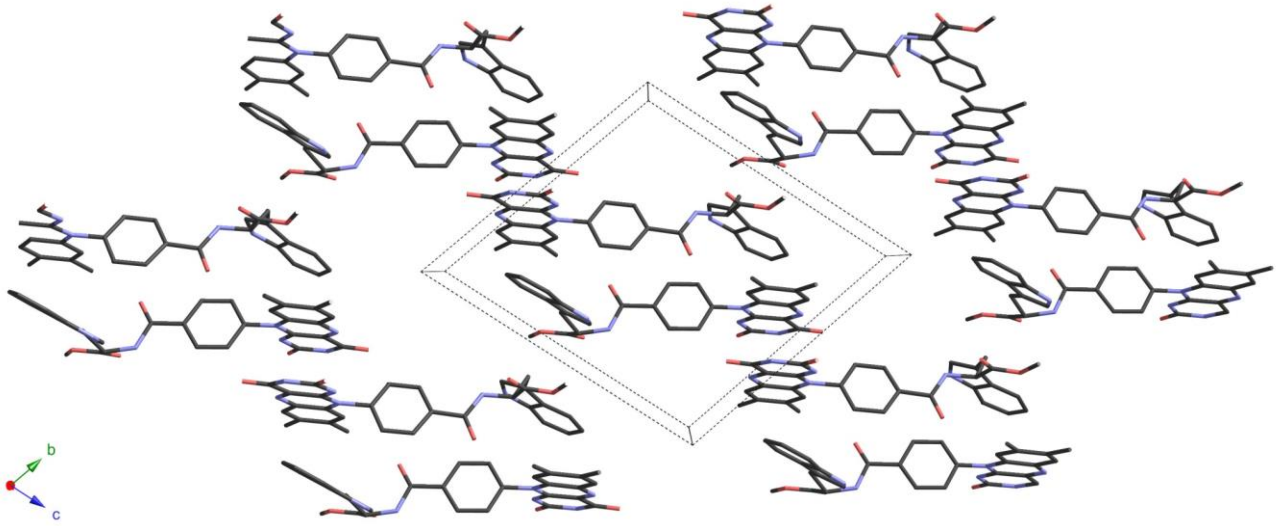

Fig. S9 3D network structure focusing on isoalloxazine and indole rings.

3. Absorption and fluorescence spectra

Absorption and fluorescence spectra were recorded on a Shimadzu UV-2600 UV-vis spectrophotometer and a HORIBA SPEX Fluorolog3-21 spectrofluorometer, respectively. The experiments were performed at 25 ºC (with a temperature controlled unit) for UV-vis and at 20 ºC (ambient temperature) for fluorescence using fresh samples. For all fluorescence spectroscopy analysis, the corrected data were used.

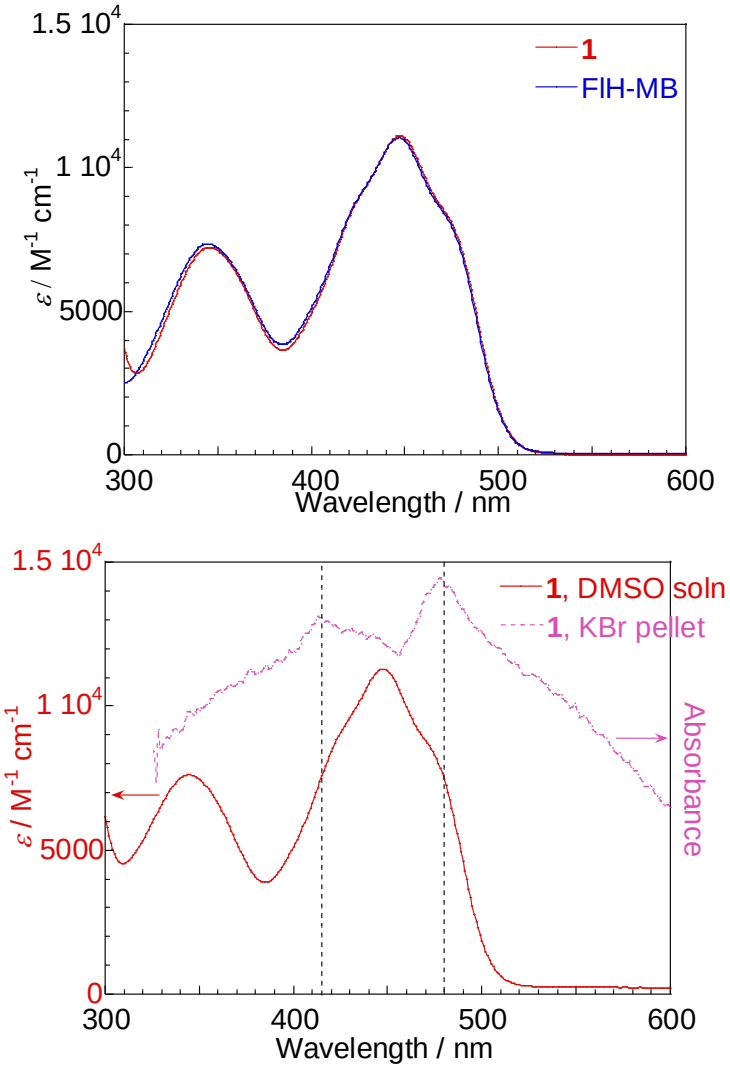

Fig. S10 Absorption spectra of **1** and FlH–MB as a reference compound. Top: 50 μM, DMSO solutions. Bottom: 100 μM, DMSO solution and KBr pellet.

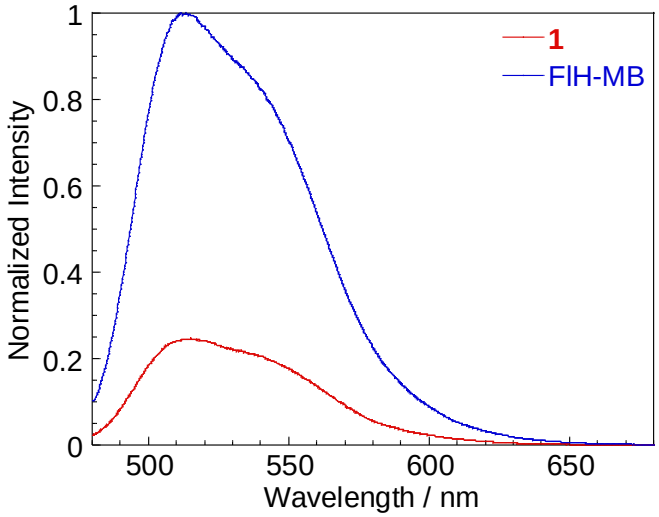

Fig. S11 Fluorescence spectra of **1** and FlH–MB as a reference compound (10 μM, DMSO solution). Excitation 450 nm.

4. Fluorescence quantum yields

For evaluation of fluorescence quantum yield, the solution of sample or standard (in a fluorescence cell with a SEPTA screw cap) was treated with Ar bubbling before use. The relative quantum yield of sample is related to that of a solution of a standard by the following equation:

$$\Phi_{F(\text{sample})} = \left(\frac{A_{\text{standard}}}{A_{\text{sample}}}\right)\left(\frac{F_{\text{sample}}}{F_{\text{standard}}}\right)\left(\frac{n_{\text{sample}}}{n_{\text{standard}}}\right)^2 \Phi_{F(\text{standard})}$$

Φ_F is the fluorescence quantum yield, A is the absorbance, F is the area under the corrected emission curve and n is the refractive index.[2] Here, $\Phi_{F(\text{sample})}$ of each solution was estimated using riboflavin as a standard material.[3]

Table S1. Fluorescence quantum yields of **1** and FlH–MB.[4]

	A	F	n	$\Phi_{F(\text{standard})}$	$\Phi_{F(\text{sample})}$
0.1 μM riboflavin/DMSO	0.00076	96480000	1.483	0.1	
0.1 μM **1**/DMSO	0.00115	15680000	1.483		0.011
0.1 μM FlH–MB/DMSO	0.00112	44490000	1.483		0.031
0.1 μM riboflavin/MeCN	0.00109	156700000	1.341	0.3	
0.1 μM **1**/MeCN	0.00116	32720000	1.341		0.059
0.1 μM FlH–MB/MeCN	0.00114	376900000	1.341		0.69

5. Fluorescence decay curves

Fluorescence decays of flavin for **1** and FlH–MB were measured with excitation by 470-nm LED light source and detection at the emission wavelength of 520 nm on a HAMAMATSU PHOTONICS Quantaurus-Tau spectrofluorometer at room temperature (~20 ºC). The solutions (in a fluorescence cell with a SEPTA screw cap) were treated with Ar bubbling before use. Total fluorescence decay F(t) is expressed by the summation of exponential decay functions with the pre-exponential factor a_i and the fluorescence lifetime τ_i for the ith component:

$$F(t) = \sum_i \alpha_i \exp(-t/\tau_i)$$

The fluorescence decay curves were fitted by non-linear least squares iterative fitting procedure.

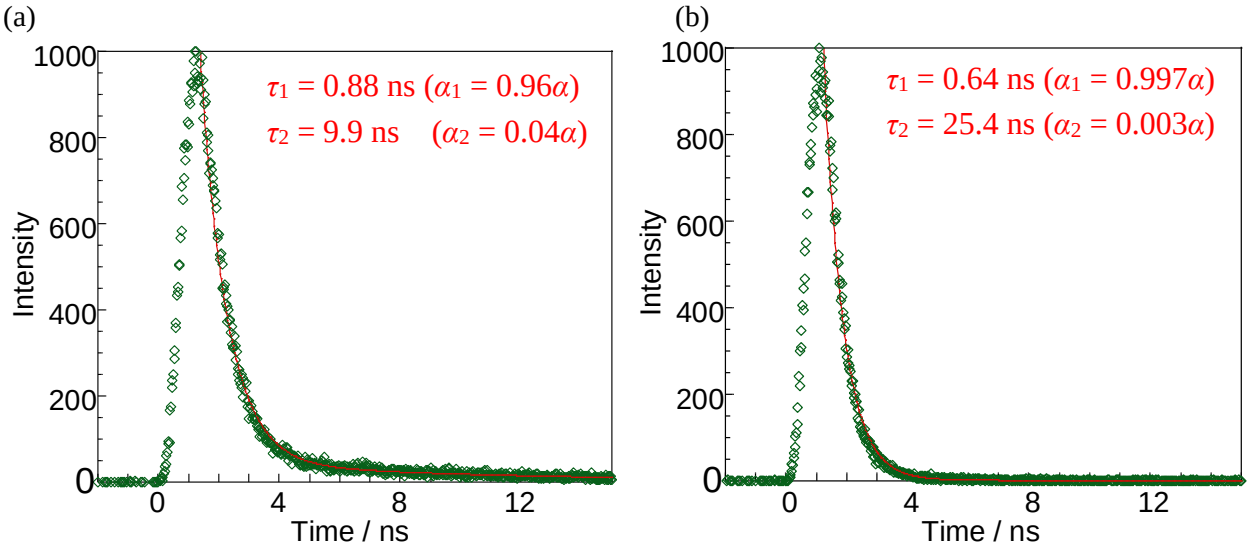

Fig. S12 Fluorescence decays of **1**. (a) 10 μM, MeCN solution, and (b) 10 μM, DMSO solution.

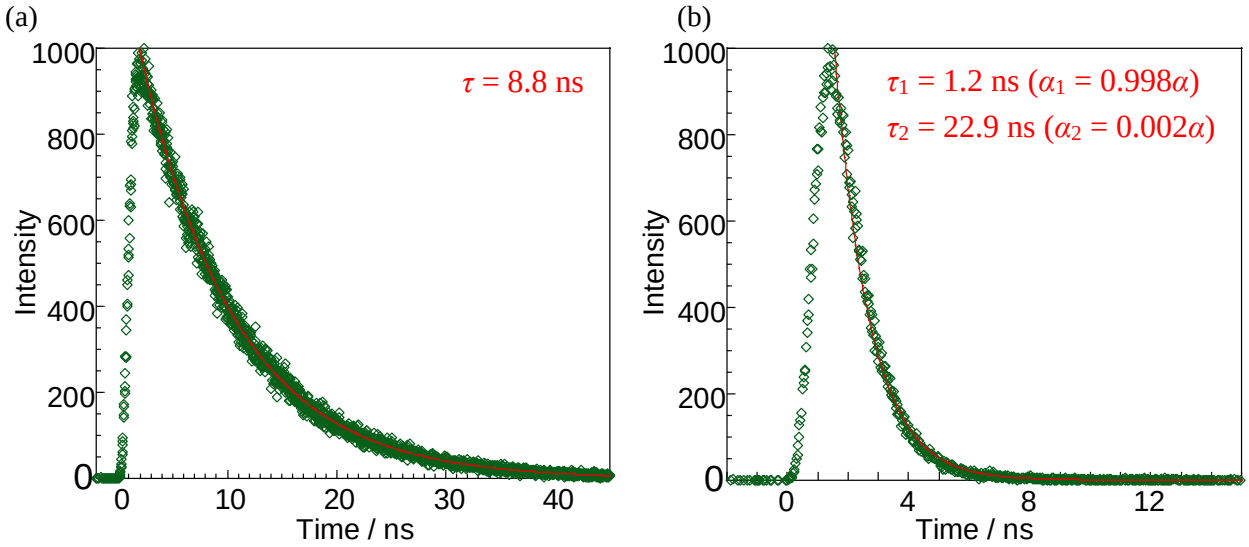

Fig. S13 Fluorescence decays of FlH–MB. (a) 10 μM, MeCN solution, and (b) 10 μM, DMSO solution.

In the case of MeCN solution, τ_1(MeCN) = 0.88 ns for **1** is much shorter than τ_0(MeCN) = 8.8 ns in FlH–MB, suggesting that the singlet quenching process occurs efficiently to generate the singlet CS state ^{1}(Fl$^{\bullet-}$–Trp$^{\bullet+}$). The singlet quenching rate constant (k_q^S) is obtained to be $k_q^S = 1/\tau_1 - 1/\tau_0 = 1.0\times10^9$ s^{-1} for **1**. Using the fluorescence quantum yield ($\Phi_{f,FlH–MB} = 0.69$) and assuming that the intersystem crossing (ISC) dominates the non-radiative deactivations in the ^{1}FlH–MB*, $k_F = \Phi_{f,FlH–MB}/\tau_0 = 7.8\times10^7$ s^{-1} (as the radiation rate of FlH–MB) and $k_{ISC} = 3.5\times10^7$ s^{-1} is obtained. The singlet quenching quantum yield is then determined to be $\Phi_q^S = k_q^S/(k_F + k_{ISC} + k_q^S) = 0.9$. This result shows that the singlet quenching reaction is major process and that only faint triplet exciton of ^{3}Fl*–Trp may be generated due to the slow ISC.

6. Concentration-dependency of fluorescence intensity

For evaluating concentration-dependency of intermolecular interaction, fluorescence spectra for the sample solutions of 0.1 μM and 10 μM were measured at room temperature (~25 ºC). Both of the entrance and exit slits were set at 5.0 nm and 1.0 nm for 0.1 μM and 10 μM samples, respectively, for efficient detection with the HORIBA SPEX Fluorolog3-21 spectrofluorometer.

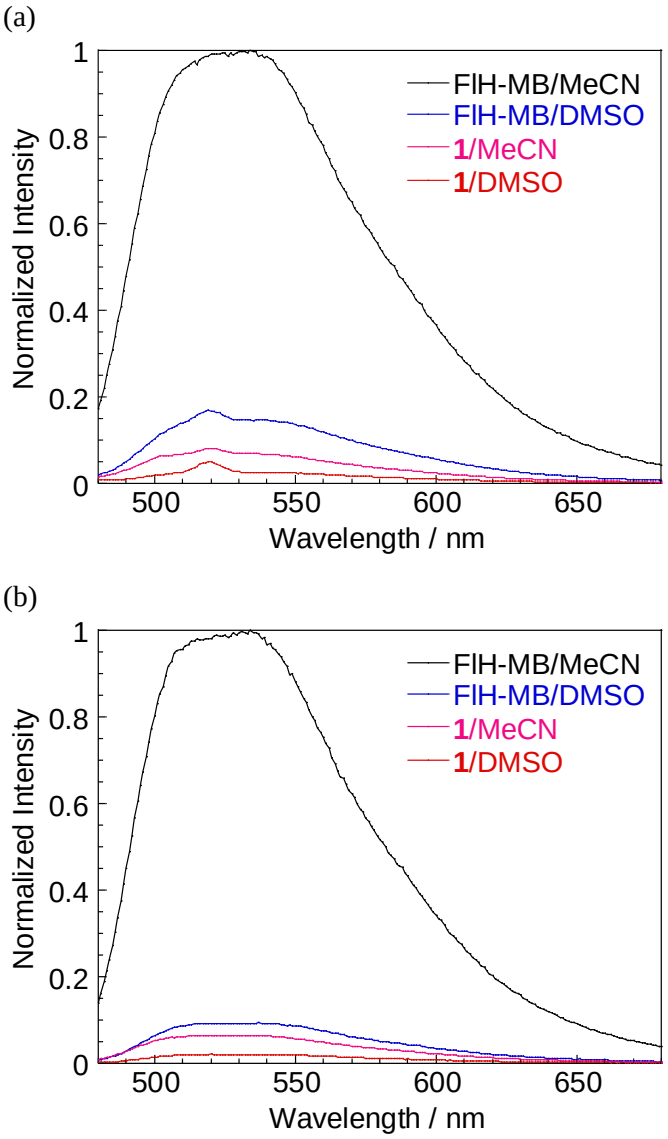

Fig. S14 Normalized fluorescence spectra of **1** and FlH–MB (in MeCN and DMSO solutions), (a) 0.1 μM and (b) 10 μM. Excitation 450 nm.

7. Temperature dependence of fluorescence quenching

Fluorescence spectra of flavin for **1** and FlH–MB were recorded on a HORIBA SPEX Fluorolog3-21 spectrofluorometer. The Fluorescence decays were measured with excitation by 470-nm picosecond laser (Spectra-Physics Quantronix Millennia-Tsunami, TITAN-TOPAS) and detection at the emission wavelength of 520 nm (by Spectral Products CM110 monochromator, PicoQuant PMA Hybrid 40 photomultiplier and TimeHarp 260 PICO TCSPC module with bandpath filter). The experiments were performed at 10, 25 and 40 ºC (with a cryostat, Unisoku CoolSpeK). The relative intensities (F) and lifetimes (τ) to those for MeCN solution of FlH–MB at 10 ºC (defined here as F_0 and τ_0) were plotted in Fig. S15.

Table S2. Fluorescence lifetimes of **1** and FlH–MB (10 μM solutions) at 10, 25 and 40 ºC. Excitation 470 nm and emission 520 nm.

	10 ºC		25 ºC		40 ºC	
	τ_1/ns	τ_2/ns	τ_1/ns	τ_2/ns	τ_1/ns	τ_2/ns
10 μM **1**/DMSO	0.42 (0.997α)	11.2 (0.003α)	0.32 (0.996α)	7.8 (0.004α)	0.29 (0.996α)	7.0 (0.004α)
10 μM FlH–MB/DMSO	1.2 (0.998α)	22.8 (0.002α)	0.91 (0.996α)	10.3 (0.004α)	0.77 (0.996α)	10.7 (0.004α)
10 μM **1**/MeCN	0.72 (0.97α)	9.0 (0.03α)	0.65 (0.97α)	8.8 (0.03α)	0.54 (0.97α)	8.0 (0.03α)
10 μM FlH–MB/MeCN	8.9	–	8.6	–	8.2	–

(a)

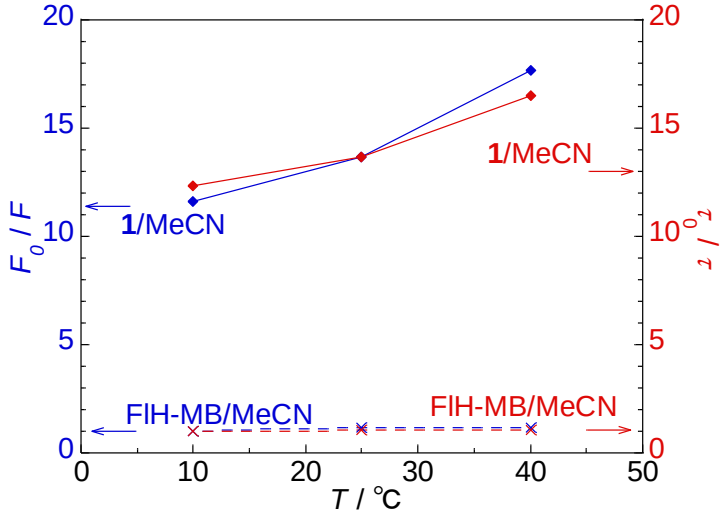

(b)

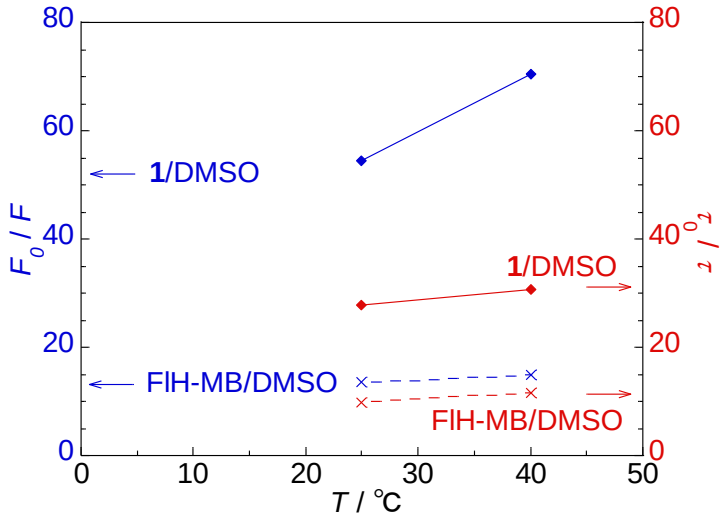

Fig. S15 Relative fluorescence intensities and lifetimes of **1** and FlH–MB (10 μM solutions). Excitation 450 nm and 470 nm for fluorescence intensity and lifetime, respectively. Emission 520 nm.

8. TREPR spectra

Sample solutions prepared at 100 μM were placed in 2 mm-quartz tubes and degassed on a vacuum line by several freeze–pump–thaw cycles. Continuous-wave (CW) TREPR measurements were performed using an X-band EPR spectrometer (Bruker E680) without field modulation. Laser pulses for sample excitation at 450 nm were prepared by using the Nd:YAG laser and MOPO system (Spectra Physics). The laser pulses and detection systems were synchronized by a Stanford Research DG535 pulse generator. The energy per pulse, pulse width, and repetition rate were 2 mJ, ~10 ns, and 30 Hz, respectively. Simulation of the polarized spectra was performed using the Matlab-based simulation tool box EasySpin.[5]

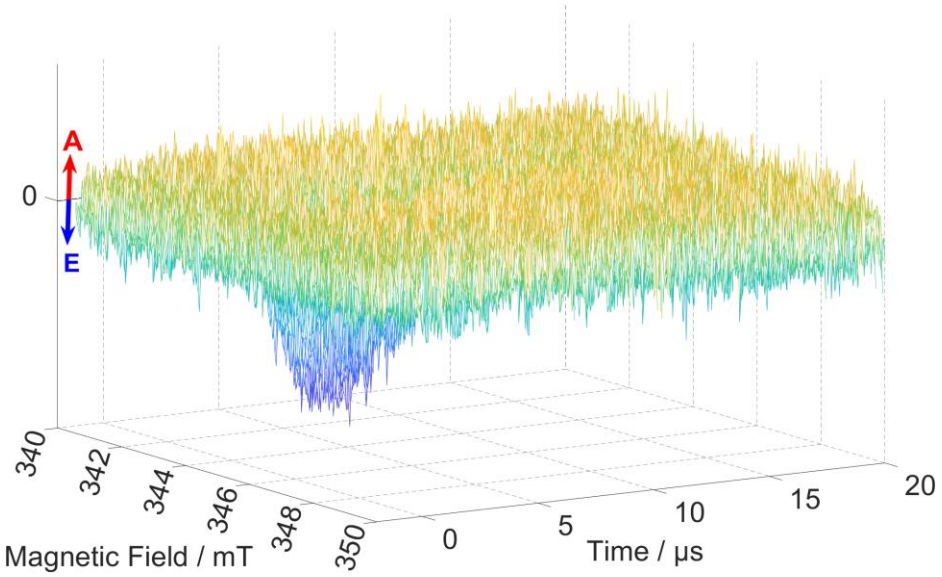

Fig. S16 3D TREPR spectrum for a 100 μM MeCN solution of **1** at 298 K (A = enhanced absorption, E = emission).

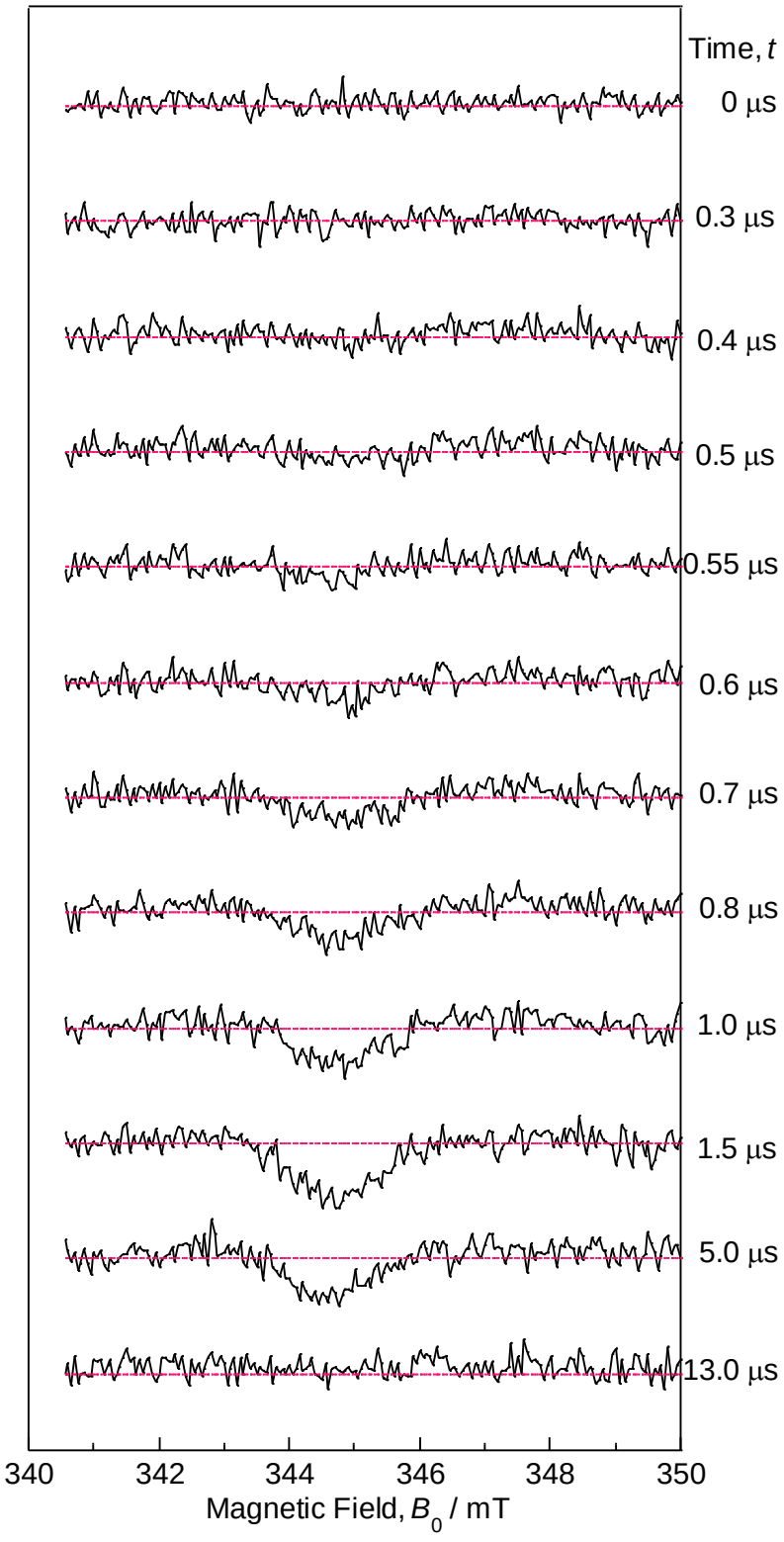

Fig. S17 Time evolution of TREPR spectra for a 100 μM DMSO solution of **1** at 298 K.

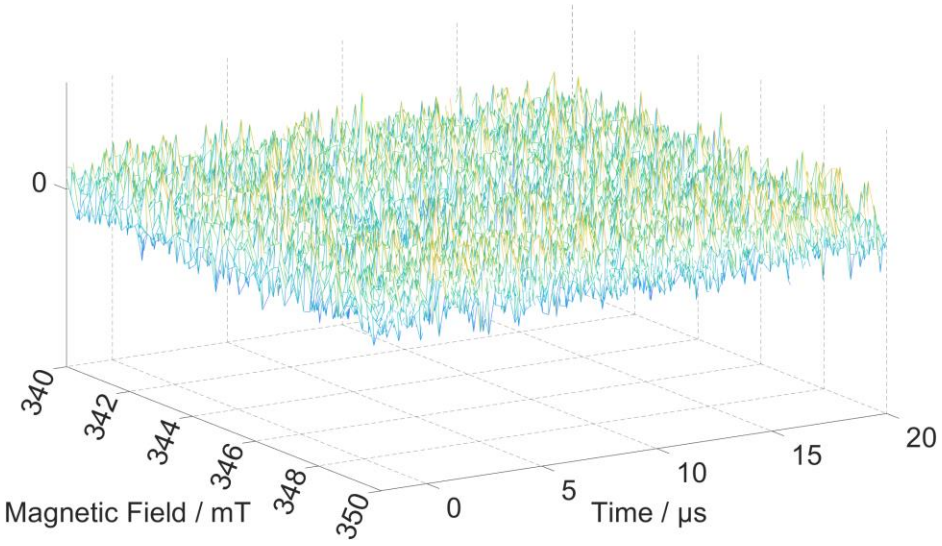

Fig. S18 TREPR spectrum for a 100 µM DMSO solution of **1** at 298 K.

9. Titration experiments of FlH–MB with tryptophan methyl ester

Fluorescence titrations with tryptophan methyl ester (Trp(OMe)) were performed at 25 ºC on a HORIBA SPEX Fluorolog3-21 spectrofluorometer. To a 10 μM DMSO solution of FlH–MB was added up to 100 μM L-tryptophan methyl ester hydrochloride (L-Trp(OMe)•HCl), which quenched the flavin fluorescence only ~5% (as shown in Fig. S17). On the other hand, titration experiment in MeCN was not possible due to the insolubility of Trp(OMe).

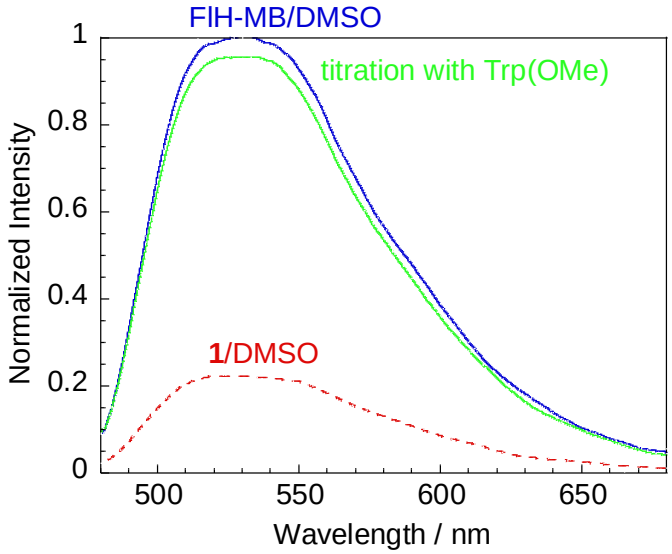

Fig. S19 Normalized fluorescence spectra of FlH–MB (10 μM, DMSO solution) titrated with Trp(OMe) (100μM). Excitation 450 nm.

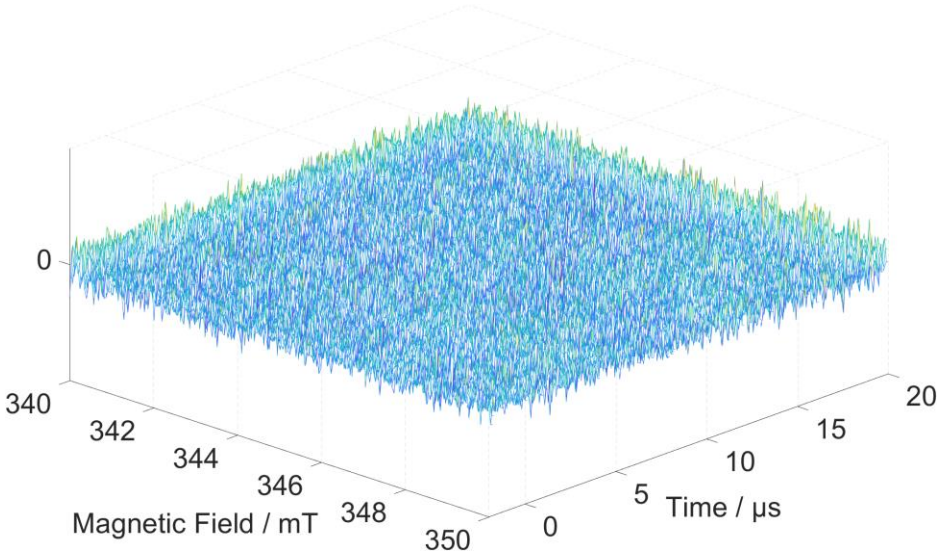

Fig. S20 TREPR spectrum of FlH‑MB (100 μM, DMSO solution) titrated with Trp(OMe) (100 μM) at 298 K.

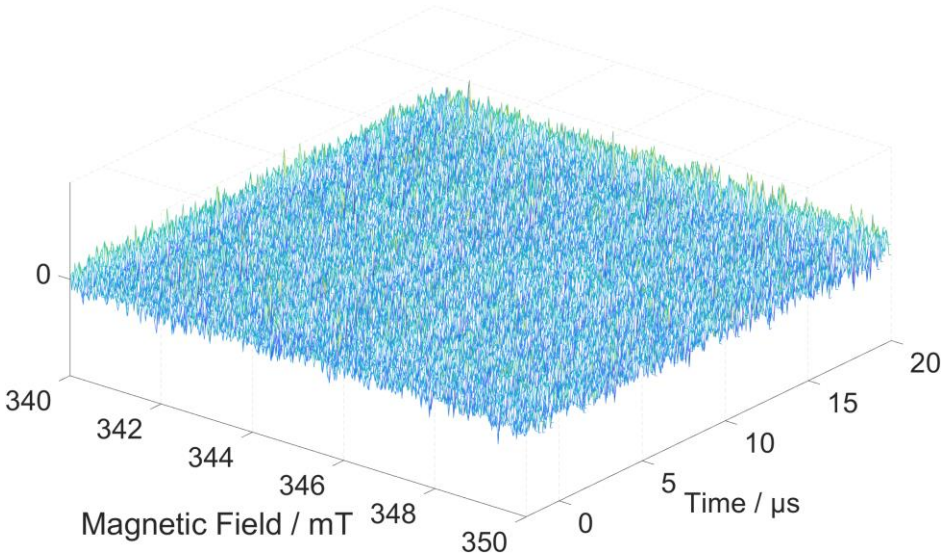

Fig. S21 TREPR spectrum of FlH‑MB (100 μM, MeCN solution) titrated with Trp(OMe) (saturated) at 298 K.

10. DFT calculations

All density functional theory (DFT) calculations were performed with the Gaussian16 program.[6] After geometry optimizations at the B3LYP/6-31G(d) level using a dyad molecule of the crystal structure as the initial structure, single point energy calculations for both the singlet ground state and the triplet excited state were performed at B3LYP/6-31+G(d,p) level. A time-dependent (TD) DFT calculation using the singlet ground state geometry was also performed at B3LYP/6-31+G(d,p) level. A polarizable continuum model (PCM) under the solvent (MeCN) field was taken into account. The results could demonstrate the reaction mechanism at least qualitatively, however, may need higher level of basis function especially during geometry optimization.

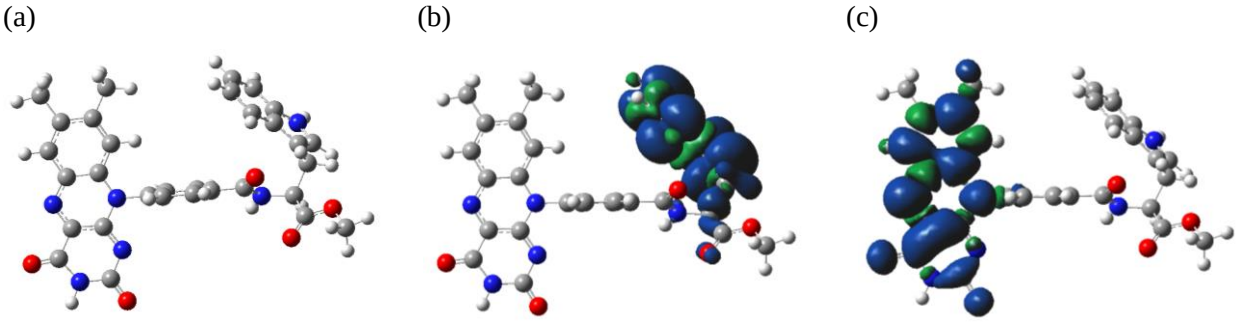

Fig. S22 (a) Optimized triplet state (T_1 state) geometry of **1** in MeCN (PCM model). Electron spin density surfaces relevant to Fig. 3; (b) radical cation of **1** and (c) radical anion of **1** in MeCN (PCM model), isovalue = 0.0004 at the optimized triplet state geometry of T_1. Blue and green colors in (b) and (c) show α and β spins, respectively.

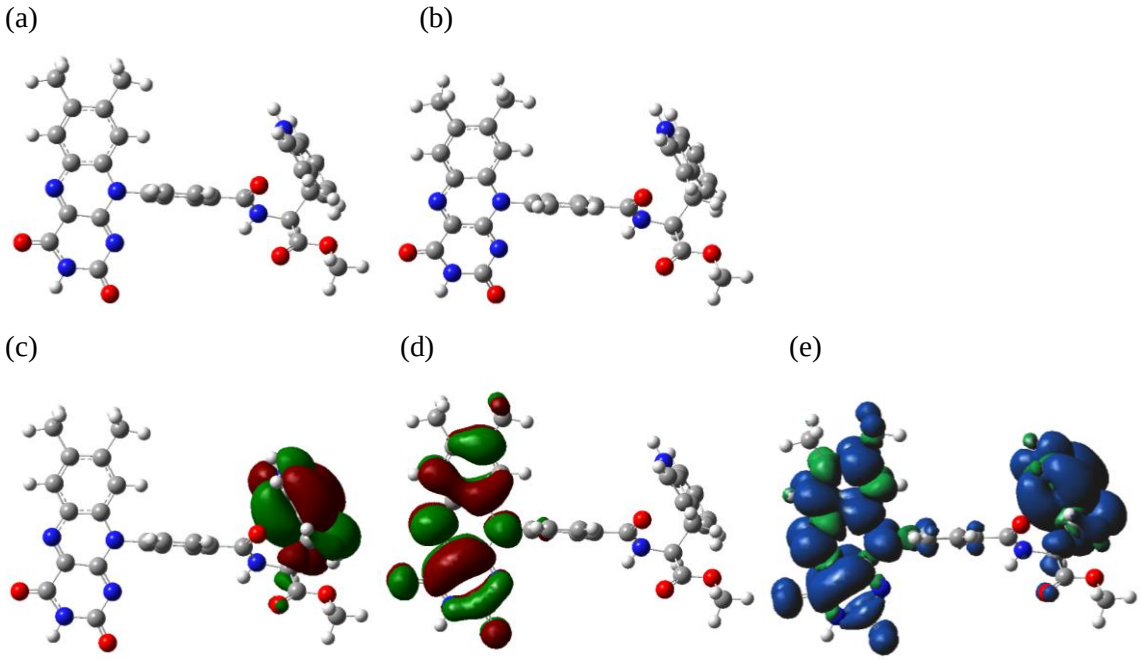

Fig. S23 (a) Optimized ground state (S_0 state) and (b) Optimized triplet state (T_1 state) geometries of **1** in vacuum. The center-to-center distances of Fl–Trp rings are 10.8 Å and 10.9 Å in (a) and (b), respectively. Frontier molecular orbitals, (c) HOMO and (d) LUMO of **1** in MeCN (PCM model), isovalue = 0.02 at the ground state geometry of S_0. (e) Electron spin density surface of the triplet state of **1** in MeCN (PCM model), isovalue = 0.0004 at the optimized triplet state geometry of T_1. Blue and green colors in (e) show α and β spins, respectively.

11. References

(1) Basel, Y.; Hassner, A. Activation of carboxylic acids as their active esters by means of *tert*-butyl 3-(3,4-dihydrobenzotriazine-4-on)yl carbonate. *Tetrahedron Lett.* **2002**, *43*, 2529–2533.

(2) Williams, A. T. R.; Winfield, S. A.; Miller, J. N. Relative fluorescence quantum yields using a computer-controlled luminescence spectrometer. *Analyst* **1983**, *108*, 1067–1071.

(3) Weigel, A.; Dobryakov, L.; Veiga, M.; Lustres, J. L. P. Photoinduced processes in riboflavin: superposition of ππ*−nπ* states by vibronic coupling, transfer of vibrational coherence, and population dynamics under solvent control. *J. Phys. Chem. A* **2008**, *112*, 12054–12065.

(4) Oka, Y. Cesium cation complexation by a flavin receptor *via* self-assembly and deprotonation. *ACS Omega* **2020**, *5*, 21226–21230.

(5) Stoll, S.; Schweiger, A. EasySpin, a comprehensive software package for spectral simulation and analysis in EPR. *J. Mag. Res.* **2006**, *178*, 42–55.

(6) Gaussian 16, Revision C.01, M. J. Frisch, G. W. Trucks, H. B. Schlegel, G. E. Scuseria, M. A. Robb, J. R. Cheeseman, G. Scalmani, V. Barone, G. A. Petersson, H. Nakatsuji, X. Li, M. Caricato, A. V. Marenich, J. Bloino, B. G. Janesko, R. Gomperts, B. Mennucci, H. P. Hratchian, J. V. Ortiz, A. F. Izmaylov, J. L. Sonnenberg, D. Williams-Young, F. Ding, F. Lipparini, F. Egidi, J. Goings, B. Peng, A. Petrone, T. Henderson, D. Ranasinghe, V. G. Zakrzewski, J. Gao, N. Rega, G. Zheng, W. Liang, M. Hada, M. Ehara, K. Toyota, R. Fukuda, J. Hasegawa, M. Ishida, T. Nakajima, Y. Honda, O. Kitao, H. Nakai, T. Vreven, K. Throssell, J. A. Montgomery, Jr., J. E. Peralta, F. Ogliaro, M. J. Bearpark, J. J. Heyd, E. N. Brothers, K. N. Kudin, V. N. Staroverov, T. A. Keith, R. Kobayashi, J. Normand, K. Raghavachari, A. P. Rendell, J. C. Burant, S. S. Iyengar, J. Tomasi, M. Cossi, J. M. Millam, M. Klene, C. Adamo, R. Cammi, J. W. Ochterski, R. L. Martin, K. Morokuma, O. Farkas, J. B. Foresman, and D. J. Fox, Gaussian, Inc., Wallingford CT, 2019.